Available online at www.sciencedirect.com
SCIENCE DIRECT®
Journal of Solid State Chemistry 170 (2003) 351–360
JOURNAL OF SOLID STATE CHEMISTRY
http://elsevier.com/locate/jssc

The metastable $Ni_{7\pm x}S_6$, and mixed $Ni_{6\pm x}(S_{1-y}Se_y)_5$, phases

Y. Liu,[a] L. Norén,[a] R.L. Withers,[a,*] J. Hadermann,[b] G. Van Tendeloo,[b] and F.J. García–García[c]

[a] *Research School of Chemistry, Australian National University, Canberra ACT 0200, Australia*
[b] *EMAT, University of Antwerp (RUCA), Groenenborgerlaan 171, B-2020 Antwerpen, Belgium*
[c] *Avdelningen för Oorganisk Kemi, Arrheniuslaboratoriet, Stockholms Universitet, S-106 91 Stockholm, Sweden*

Received 16 July 2002; received in revised form 1 October 2002; accepted 7 October 2002

Abstract

The closely related, narrowly non-stoichiometric, metastable as well as thermodynamically stable "phases" in the metal-rich part of the Ni–S phase diagram near the nominal composition $Ni_{7\pm x}S_6$ have been carefully re-investigated via electron diffraction and transmission electron microscope imaging. Two quite distinct polymorphs have been identified, a minority incommensurate interface-modulated polymorph and a (heavily twinned) majority $I1a1$, $\mathbf{a}=2\mathbf{a}_p$, $\mathbf{b}=2\mathbf{b}_p$, $\mathbf{c}=-\mathbf{a}_p+\mathbf{c}_p$ superstructure (of an underlying *Bmmb*, $a_p\sim3.3$, $b_p\sim16.4$, $c_p\sim11.3$ Å parent structure) polymorph. The incommensurate polymorph is shown to be very closely related to the only known polymorph of $Ni_{6\pm x}Se_5$ and is rapidly stabilized to room temperature upon doping of the sulfide compounds with selenium.

Keywords: $Ni_{7\pm x}S_6$; Metastable phases; TEM study

1. Introduction

There exist several closely related, narrowly non-stoichiometric, metastable as well as thermodynamically stable "phases" in the metal-rich part of the Ni–S and Ni–Se phase diagrams [1–13] near the nominal composition $Ni_{7\pm x}X_6$ (X=S, Se). These phases are intriguing because of the apparent ease of Ni diffusion within the chalcogenide substructure but are to date still rather poorly understood from the crystallographic point of view. The high-temperature thermodynamically stable phases exist only over a limited temperature interval (400–570°C and 450–670°C for the sulfide and selenide, respectively [4,11,12], but can apparently be "stabilized" to room temperature either via rapid quenching or via doping of S with Se in the case of $Ni_{7\pm x}S_6$ or of Se with Te in the case of $Ni_{7\pm x}Se_6$ [4,5].

In the case of the selenide, a recent transmission electron microscope (TEM) study of the quenched material found a single, incommensurate (in general) interface-modulated, $Ni_{6\pm x}Se_5$ solid solution phase [13]. In the case of the sulfide material, however, up to four quite distinct metastable phases, or mixtures thereof, can apparently be obtained dependent upon the quench rate, or from the as-quenched material via appropriate, surprisingly low-temperature heat treatment [11,12]. The average, or parent, structure in each case appears to be orthorhombic *Bmmb* with cell dimensions $a_p\sim3.3$, $b_p\sim16.4$, $c_p\sim11.3$ Å [5,7] (see Fig. 1). Density measurements suggest that this average structure unit cell always contains 20 sulfur atoms whereas the number of Ni atoms is able to vary within certain limits around 23–24 per unit cell [1,2,5,7]. (Clearly, Ni ion diffusion is remarkably facile in these materials). The only average structure refinement of Ni_7S_6 [7] is largely consistent with this idea of a well-defined, essentially fully occupied sulfur array into some of the various interstices of which are fitted the required number of Ni atoms (see Fig. 1).

Two out of the five Ni atom sites in the Ni_7S_6 average structure refinement were essentially fully occupied while each of the remaining three sites were approximately one-half occupied (7) (see Fig. 1b). Simultaneous local occupancy of various of these partially occupied Ni sites in the underlying average structure is precluded by Ni–Ni contact distances which are unphysical (see, for

*Corresponding author. Fax: +26-12-507-50.
E-mail address: withers@rsc.anu.edu.au (R.L. Withers).

0022-4596/03/$ - see front matter © 2002 Elsevier Science (USA). All rights reserved.
doi:10.1016/S0022-4596(02)00123-8

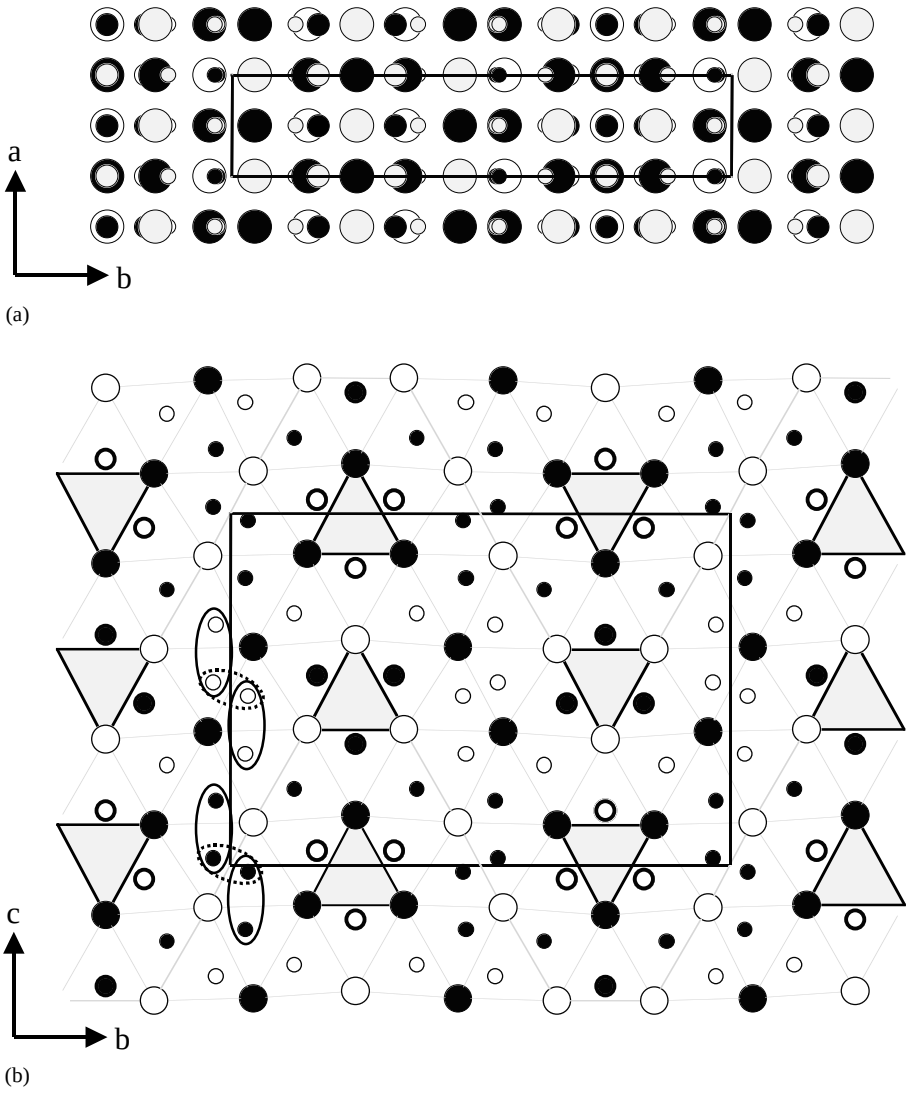

Fig. 1. Shows (a) the refined average structure of Ni_7S_6 [7] projected onto the a–b plane. The S atoms are depicted by the large circles, the Ni atoms with approximately full occupancy by the medium-size circles and the Ni-atoms with $\sim 50\%$ occupancy by the small circles. Unfilled circles are found in the bottom $\sim\frac{1}{3}$ of the projection axis ($0 \leqslant z \leqslant \frac{1}{3}$), black circles in the middle $\frac{1}{3}$ and grey circles in the remaining $\frac{1}{3}$ closest to the viewer. The same structure is shown projected onto the b–c plane in (b). Unfilled symbols are at the height $x = 0$ while the filled symbols are at the height $x = \frac{1}{2}$. Some of the $\sim 50\%$-occupied Ni-atoms have been circled in pairs in (b) to show that these pairs of Ni atoms have unnaturally short interatomic separation distances and hence cannot be simultaneously occupied.

example, the circled pairs of Ni atoms in Fig. 1b). This provides a rationale or justification of the need for additional occupational modulation and associated structural relaxation giving rise to weak satellite reflections in addition to the strong parent reflections **G** corresponding to the above average structure unit cell.

The crystallography (unit cell/s, space group symmetry/ies, etc.) of these modulated metastable phases, however, remains largely unclear, particularly in the case of the sulfides, and is the principal subject of the present contribution. Given the metastability and documented sensitivity of the sulfide compounds to thermal history (12), it was decided to also investigate the pseudo-binary Ni_6S_5–Ni_6Se_5 solid solution in an attempt to stabilize one or other of the reported higher temperature polymorphs. We begin with a survey of previously obtained diffraction results.

1.1. Previous diffraction results

The earliest TEM study [9] reported a sequence of $[012]_p$ (p for parent) electron diffraction patterns (EDPs) providing evidence for at least four distinct types of superstructures as a function of decreasing temperature. The highest temperature polymorph was reported to be characterized by pairs of satellite reflections " .. about the absent $h+k+l=$ odd positions, with the separation of the pairs in the a^* direction .. " [9]. It is worth noting here that Fleet [7] also reported that ".. zero-level, c-axis

precession films of α-Ni_7S_6 generally show weak superstructure reflections with non-integral spacings in the **a*** direction….'' Such descriptions are strongly reminiscent of the reciprocal lattice of the incommensurate interface modulated structure recently reported for $Ni_{6\pm x}Se_5$ (see Fig. 2 of [13] and below). On subsequent further lowering of temperature, Putnis [9] reported ".. a transitory 4*a*, 1*b*, 1*c* superstructure ... before transformation to a 2*a*, 2*b*, 2*c* superstructure .. generally associated with a certain amount of disorder shown as streaking .. parallel to *b** .. '' before a final transformation to a 2*a*, 3*b*, 3*c* superstructure which was reported to be the lowest temperature state.

More recently, Hansen et al. [10] reported an electron diffraction study of $Ni_{1.155}S$ and $Ni_{1.135}S$ samples annealed at 100°C and 200°C, respectively, before quenching. A monoclinic $Ni_{7\pm x}S_6$-type polymorph ($\mathbf{a}=-\mathbf{a}_p+\mathbf{c}_p$, $\mathbf{b}=-2\mathbf{b}_p$, $\mathbf{c}=2\mathbf{a}_p$, reported space group *Pm*) labelled α was found in the 100°C-annealed specimen while a very similar polymorph (except for the existence of strong diffuse streaking along the *b** direction) labelled α′ was found in the 100°C-annealed specimen [10].

Finally, Stølen et al. [11] and Seim et al. [12] reported the existence of four quite distinct polymorphs (α^{i}, α^{ii}, α^{iii} and α^{iv}), largely from very careful calorimetric and XRD studies. It was reported that the α^{i} polymorph was ".. strongly related to the (unstable) as-quenched state .." which, on storing at room temperature transformed to the α^{iv} polymorph. On heating, quasi-reversible phase transformations to the α^{ii} and α^{i} polymorphs were observed although it was stated that the ".. actual phase sequence observed … depends strongly on the thermal history of the sample and especially on the heating rate .." [12]. The formation of the α^{iii} polymorph was reported to require long annealing times at ~ 350 K [12].

From the structural characterization point of view, Seim et al. [12] reported $\mathbf{a}(\alpha^{ii})=2\mathbf{a}_p$, $\mathbf{b}(\alpha^{ii})=2\mathbf{b}_p$, $\mathbf{c}(\alpha^{ii})=-\mathbf{a}_p+\mathbf{c}_p$ ($a=6.238(1)$ Å, $b=32.83$, $c=11.596$ Å; $\beta=101.83°$) for the α^{ii} polymorph. No space group, however, was given. The *b*-axis for the α^{i} polymorph was reported to be ".. half of that for α^{ii}, whereas the monoclinic lattice of α^{iv} is probably the same as that of α^{ii}..''.

2. Experimental

2.1. Synthesis

Samples of nominal composition Ni_7S_6 and Ni_6S_5 were prepared from Ni and S powders reacted together in a sealed silica tube. The reaction was carried out at 600°C since the gas pressure of S otherwise might cause the silica tube to explode. The reacted material from this procedure was then quenched in water, annealed at

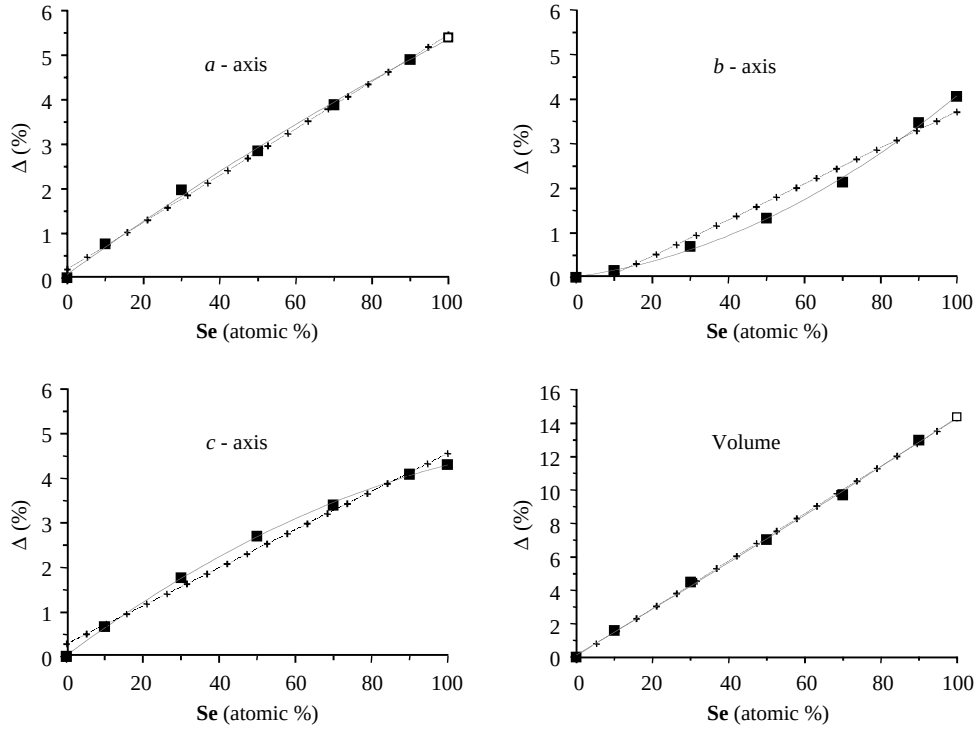

Fig. 2. Shows the variation in unit-cell parameters and volume (in the form of a percentage change relative to the starting value) across the ''pseudo-binary'' Ni_6S_5–Ni_6Se_5 system as a function of selenium content. The unfilled squares for the 100% Se sample indicate that the obtained values were obtained from those refined for a $2\times1\times1$ superstructure. The data are fitted with a linear regression (hatched line and crosses) and second-order polynomial (continuous line). The deviation from linearity is small and the system obeys Vegard's law for a solid solution.

730°C for a further 4 days followed again by water quenching. The resultant material was then ground, pressed into pellets and re-annealed at 570°C and 615°C for a week. This procedure was repeated until the X-ray powder patterns, which were taken after each annealing period, remained unchanged. The typical annealing time was 3 weeks. At this point, the reaction was assumed to have reached completion. All heat treatments were performed in evacuated silica tubes. Ni_6Se_5 was prepared in like fashion (see [13] for details).

Samples in the ternary $Ni_6(S_{1-y}Se_y)_5$ system were made by mixing stoichiometric amounts of both Ni_6S_5 and Ni_6Se_5, then thoroughly grinding them together in a mortar. The resultant mixture was then pressed into pellets and sealed in evacuated quartz tubes and heat treated at 460°C. This procedure was repeated periodically until the X-ray powder patterns, which were taken after each annealing period, remained unchanged. The total annealing time was typically 6 weeks.

2.2. X-ray powder diffraction

The average structure unit-cell dimensions of the various samples were investigated using a Guinier–Hägg camera. Silicon ($a = 5.4310280$ Å at 22.5°C [14]) was used as an internal standard and the corrected diffraction lines were refined with a least-squares program.

2.3. TEM

The samples used in the TEM investigations were prepared by carefully grinding them under butanol followed by dispersal onto holey-carbon copper grids. The samples were examined using a Philips EM 430 TEM. High-resolution electron microscopy (HREM) was carried out on a JEOL 4000EX TEM.

3. Results and discussion

3.1. X-ray powder diffraction

The refined average structure cell dimensions of the as-prepared Ni_6S_5 sample were determined to be orthorhombic with lattice parameters $a = 3.2568(2)$ Å, $b = 16.4311(10)$ Å, and $c = 11.3380(5)$ Å, while those of Ni_6Se_5 were $a = 6.8651(5)$ Å, $b = 17.0975(9)$ Å, and $c = 11.8255(8)$ Å. These are in good agreement with previously published results. The refined average structure unit-cell dimensions of the $Ni_6(S_{1-y}Se_y)_5$ samples as a function of Se content, y, are found in Table 1 and shown in the form of a percentage deviation away from the corresponding value for $y = 0$ in Fig. 2.

The $y = 0$ and 0.10 samples both show traces of Ni_3S_2, decreasing with increasing amount of selenium. This agrees with the data from, amongst others, Seim et al. [12] which show that the maximum nickel content in the sulfide at ~460°C is $Ni_{5.96}S_5$, i.e., a second more Ni-rich phase must also be present for Ni_6S_5, in small amounts. In the Ni_6Se_5 sample, traces of NiSe were observed indicating that the nominal Ni_6Se_5 compound is at the metal-poor end of the $Ni_{6\pm x}Se_5$ solid solution. Increasing the radii of the "average chalcogenide" apparently allows more nickel to be incorporated into the chalcogen array/structure.

3.2. TEM investigation of the quenched Ni_7S_6 and Ni_6S_5 specimens

At least two quite distinct polymorphs were identified in our quenched material, frequently intergrown on a relatively fine scale (see Fig. 3), particularly in specimens observed soon after synthesis. One of these polymorphs, very much the minority phase in our quenched material, was rather unstable on storing at room temperature and appeared to vanish altogether in specimens held at room temperature for any significant length of time. We therefore identify this particular polymorph with the as-quenched material of Seim et al. [12] which was also reported to be rather unstable on storing at room temperature, as well as being strongly related to the α^i polymorph.

Fig. 3a shows a typical $[001]_p$ zone axis EDP taken from an area including this as-quenched material along with a corresponding low-magnification image of the area from which the EDP in (a) was taken. Note the ~30–40 Å fringes running perpendicular to $\mathbf{a}_p$ which

Table 1
Refined unit cell parameters for $Ni_6(S_{1-x}Se_x)_5$ compounds

x	a (Å)	b (Å)	c (Å)	V (Å^3)
0*	3.2568(2)	16.4311(10)	11.3380(5)	606.74(6)
0.1*	3.2816(3)	16.4559(14)	11.4139(9)	616.37(9)
0.3	3.3211(4)	16.5443(16)	11.5386(10)	633.99(11)
0.5	3.3515(8)	16.642(4)	11.634(3)	648.9(3)
0.7	3.3832(6)	16.782(5)	11.723(3)	665.6(3)
0.9	3.4163(7)	17.002(3)	11.8015(10)	685.5(2)
1.0#	6.8651(5)	17.0975(9)	11.8255(8)	1388.0(2)

Two phase samples with traces of Ni_3S_2 marked with an "" and with traces of NiSe with a "#".

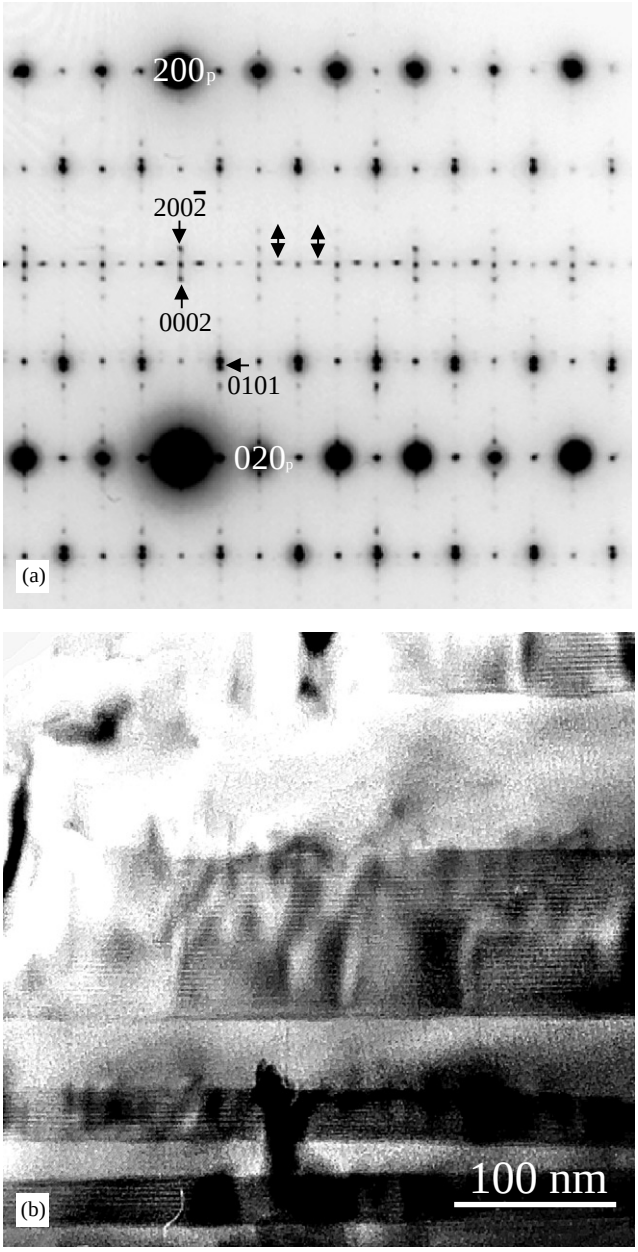

Fig. 3. Shows (a) a typical $[001]_p$ zone axis EDP from an area including the minority as-quenched phase in the "Ni_7S_6" sample while (b) shows the corresponding aligned low-magnification image of the same area. Note the lamellar domains and the ~30–40 Å fringes running perpendicular to a_p which disappear in alternate lamellae in (b). Clearly, the EDP shown in (a) is not from a "single-phase" region, despite there being no obvious evidence of splitting in the parent, e.g., $[200]^*_p$ or $[020]^*_p$, Bragg reflections of (b).

disappear in alternate lamellae in (b). Clearly, the EDP shown in Fig. 3a is not from a "single-phase" region, despite there being no obvious evidence of splitting in the parent, e.g., $[200]^*_p$ or $[020]^*_p$, Bragg reflections. Fig. 3a is nonetheless clearly strongly reminiscent of the equivalent $[001]_p$ zone axis EDP of the incommensurate interface-modulated Ni_6Se_5 structure (cf., for example, Fig. 3a with Fig. 2a of [13]), exhibiting characteristic pairs of incommensurate satellite reflections split along the parent a^*_p reciprocal lattice direction (see, for example, the reflections labelled 0002 and $200\bar{2}$ in Fig. 3a) in much the same way as described above for the highest temperature α^i polymorph by Putnis [9] and for α-Ni_7S_6 by Fleet [7], as well as for Ni_6Se_5 in [13]. (Note that the four–integer indexation in Fig. 3a is with respect to the reciprocal space basis vector set $\mathbf{M}^* = \{\mathbf{a}^*_p, \mathbf{b}^*_p, \mathbf{c}^*_p, \mathbf{q} = (\frac{1}{2} - \varepsilon)\mathbf{a}^*_p$ with $\varepsilon \sim 0.03-0.04\}$).

We therefore identify the as-quenched material of Seim et al [12] as well as the α^i polymorph with the (in general) incommensurate interface-modulated structure-type polymorph recently described for $Ni_{6\pm x}Se_5$ [13]. Unfortunately, the difficulty in finding this particular polymorph in conjunction with its strongly intergrown nature when discovered makes it difficult to definitively identify.

In addition to the incommensurate satellite reflections described above, note that Fig. 3a also shows two types of satellite reflections which are not present in Fig. 2a of [13]. The first type correspond to putting ε to zero in the above basis vector set, i.e., to the incommensurate primary modulation wave-vector $\mathbf{q}$ locking in to $\frac{1}{2}\mathbf{a}^*_p$ exactly (cf., for example, Fig. 3a with Figs. 3a and 2a of [13]). A locked-in state was also observed for $Ni_{6\pm x}Se_5$, even in specimens with the same nominal composition [13]. Commensurate and incommensurate regions were never intergrown, however, in the case of the selenide on such a fine scale that the corresponding commensurate and incommensurate satellite reflections were necessarily simultaneously observed. This has, however, been observed on several occasions in the current case and may reflect quenched-in slight compositional inhomogeneities. The second type of satellite reflections which are present in Fig. 3a but not in Fig. 2a of [13] correspond to $\mathbf{G} \pm \frac{1}{2}[210]^*_p$-type satellite reflections (see the reflections pointed to by the double-headed arrows in Fig. 3a) and belong to the (by far) majority polymorph identified in our quenched material (cf. with Fig. 4b).

The majority phase, presumably the α^{iv} polymorph given the results of Seim et al. [12], was far more easily identified and representative EDPs obtained. Fig. 4, for example, shows (a) $[100]_p$, (b) $[001]_p$ and (c) $[010]_p$ EDPs typical of this polymorph. (d) is an EDP obtained by tilting a few degrees away from the exact $[010]_p$ zone axis orientation of (c) keeping $[200]^*_p$ excited in order to bring up weak superstructure reflections in Higher Order Laue Zone (HOLZ) rings. The *Bmmb*-allowed parent Bragg reflections are indexed with a subscript p. Indexation without the subscript p is with respect to the cell reported for the α^{ii} (and α^{iv}) polymorphs by Seim et al. [12] as well as Hansen et al. [10] (albeit in a different setting), i.e., $\mathbf{a} = 2\mathbf{a}_p$, $\mathbf{b} = 2\mathbf{b}_p$, $\mathbf{c} = -\mathbf{a}_p + \mathbf{c}_p$ ($\mathbf{a}^* = \frac{1}{2}[101]^*_p$, $\mathbf{b}^* = \frac{1}{2}[010]^*_p$, $\mathbf{c}^* = [001]^*_p$). (Such a cell is

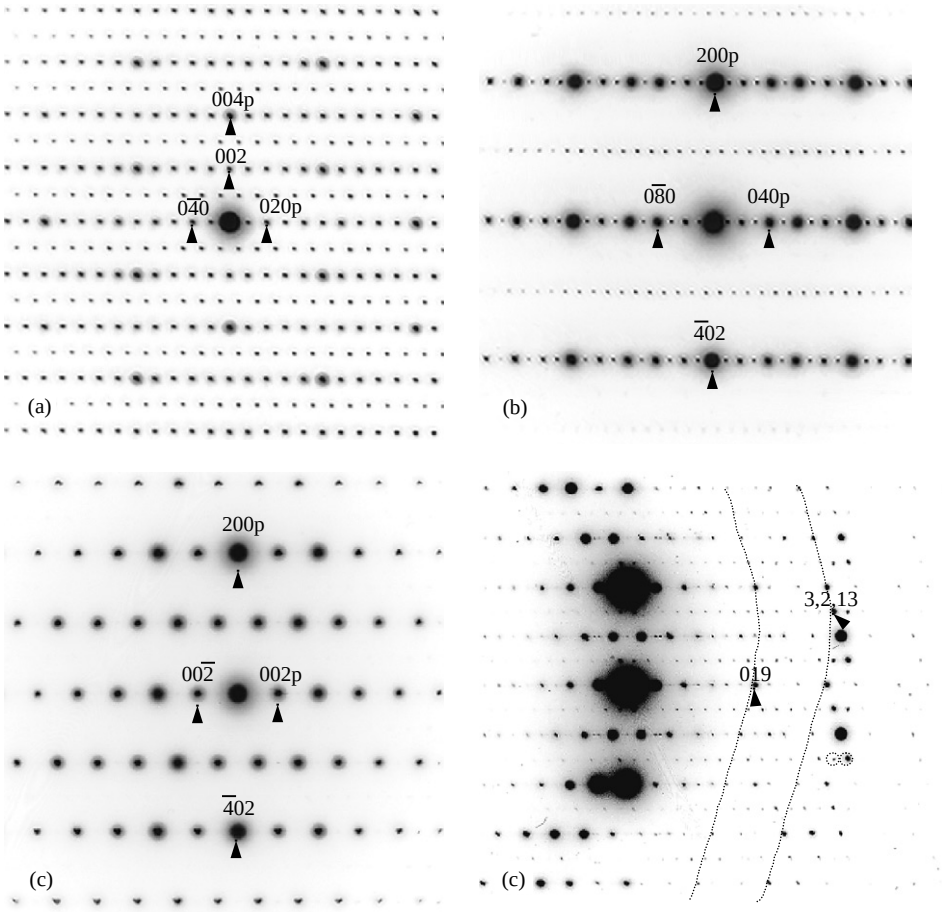

Fig. 4. Shows (a) $[100]_p$, (b) $[001]_p$ and (c) $[010]_p$ EDPs typical of the majority polymorph found in both the "Ni_7S_6" and "Ni_6S_5" samples. (d) is an EDP obtained by tilting a few degrees away from the exact $[010]_p$ zone axis orientation of (c) keeping $[200]^*_p$ excited in order to bring up weak superstructure reflections in HOLZ rings. The *Bmmb*-allowed parent Bragg reflections are indexed with a subscript p. Indexation without the subscript p is with respect to the cell reported for the α^{ii} (and α^{iv}) polymorphs by Seim et al. [12] as well as Hansen et al. [10] (albeit in a different setting), i.e., $\mathbf{a}=2\mathbf{a}_p$, $\mathbf{b}=2\mathbf{b}_p$, $\mathbf{c}=-\mathbf{a}_p+\mathbf{c}_p$ ($\mathbf{a}^*=\frac{1}{2}[101]^*_p, \mathbf{b}^*=\frac{1}{2}[010]^*_p, \mathbf{c}^*=[001]^*_p$).

also consistent with the 2*a*, 2*b*, 2*c* superstructure reported by Putnis [9]).

Note the presence of additional $\mathbf{G}\pm\frac{1}{2}[012]^*_p \equiv \mathbf{G}\pm\frac{1}{2}[210]^*_p$-type satellite reflections in the Zero(OLZ)'s of (a) and (b) as well as the presence of $\mathbf{G}\pm\frac{1}{2}\langle 101\rangle^*_p$-type satellite reflections (such as the circled pair of satellite reflections) in the Second(OLZ) of (d). The latter $\mathbf{G}\pm\frac{1}{2}\langle 101\rangle^*_p$-type satellite reflections are forbidden from appearing in the ZOLZ of $[010]_p$ EDPs by an *a* glide perpendicular to **b** (see Fig. 4c). Note further that the intensity of the right-hand-circled $\mathbf{G}\pm\frac{1}{2}[10\bar{1}]^*_p$-type satellite reflection in the SOLZ of Fig. 4d is clearly significantly stronger than that of the left-hand circled $\mathbf{G}\pm\frac{1}{2}[101]^*_p$-type satellite reflection. The relative intensities of such pairs of satellite reflections were observed to vary significantly upon slight movement of the electron probe suggesting the presence of fine-scale twinning whereby only one or other type of $\mathbf{G}\pm\frac{1}{2}\langle 101\rangle^*_p$ satellite reflection is ever locally present. The same effect was also observed in the ZOLZ of EDPs taken at zone axes such as $\langle 01\bar{1}\rangle_p$ (see Fig. 5d) where the relative intensities of $\mathbf{G}\pm\frac{1}{2}[1\bar{1}1]^*_p$ satellite reflections (such as that labelled 110 in Fig. 5d) and $\mathbf{G}\pm\frac{1}{2}[1\bar{1}\bar{1}]_p$-type satellite reflections also varied significantly upon slight movement of the electron probe again suggesting the presence of fine-scale twinning.

This is also strongly suggested by the variability in detail of, for example, $\langle 101\rangle_p$-type zone axis EDPs observed for this polymorph (cf. for example Fig. 5a with b). Note the apparent simultaneous presence of $\mathbf{G}\pm\frac{1}{2}[10\bar{1}]^*_p$-as well as $\mathbf{G}\pm\frac{1}{2}[11\bar{1}]^*_p$-type satellite reflections in (b) but the apparent absence of the latter combined with the presence of heavy diffuse streaking running along *b** through the satellite reflections in (a). Similar variability and EDPs have also been reported by Hansen et al. [12] but interpreted differently in terms of distinct (α' and α'') polymorphic forms. Note that the genuine simultaneous presence of $\mathbf{G}\pm\frac{1}{2}[10\bar{1}]^*_p$-as well as $\mathbf{G}\pm\frac{1}{2}[11\bar{1}]^*_p$-type satellite reflections in (b) would necessitate a *P* Bravais lattice and is presumably responsible for

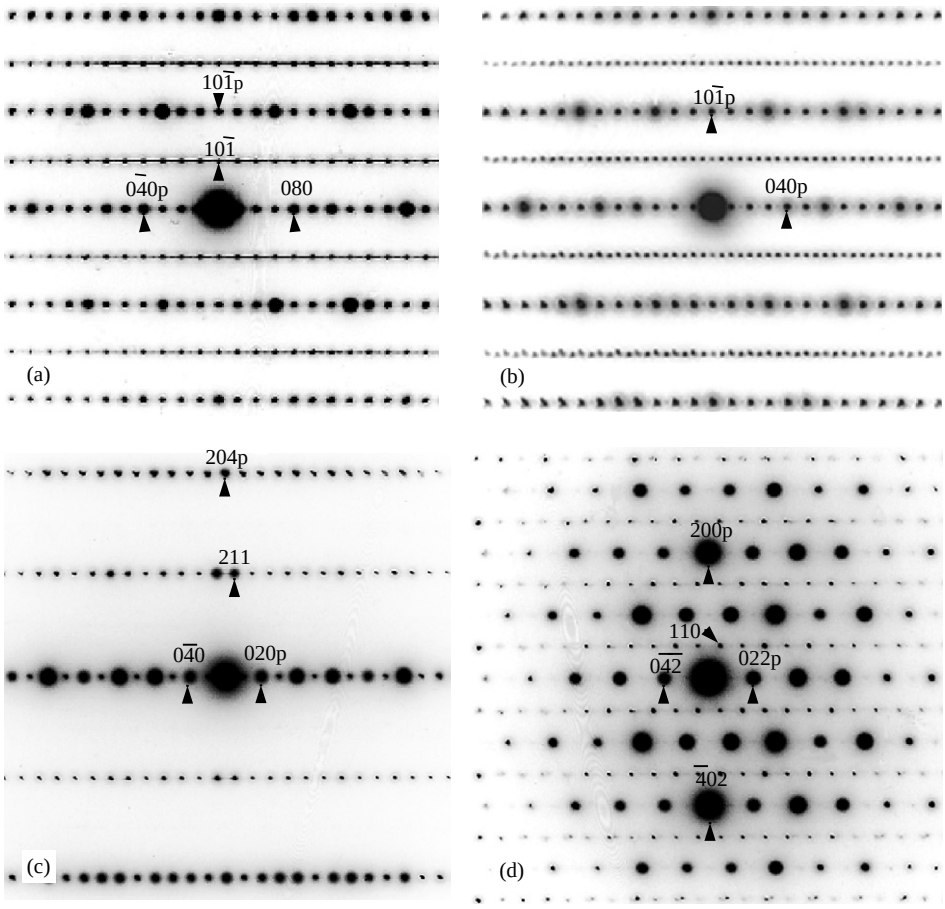

Fig. 5. Shows (a) and (b) $[101]_p$, (c) $[20\bar{1}]_p$ and (c) $[01\bar{1}]_p$ EDPs typical of the majority polymorph found in both the "Ni_7S_6" and "Ni_6S_5" samples. The *Bmmb*-allowed parent Bragg reflections are indexed with a subscript p. Indexation without the subscript p is with respect to the cell $\mathbf{a}=2\mathbf{a}_p$, $\mathbf{b}=2\mathbf{b}_p$, $\mathbf{c}=-\mathbf{a}_p+\mathbf{c}_p$ ($\mathbf{a}^*=\frac{1}{2}[101]^*_p, \mathbf{b}^*=\frac{1}{2}[010]^*_p, \mathbf{c}^*=[001]^*_p$).

the *Pm* space group reported for α'' by Hansen et al. [10]. Such a space group cannot be correct both because it neglects the above evidence for twinning as well as the characteristic systematic extinction condition observed in Fig. 4c.

The only interpretation consistent with all of the above diffraction evidence is that the polymorph is characterized by variable, often fine-scale, twinning of an $\mathbf{a}=2\mathbf{a}_p$, $\mathbf{b}=2\mathbf{b}_p$, $\mathbf{c}=-\mathbf{a}_p+\mathbf{c}_p$ ($\mathbf{a}^*=\frac{1}{2}[101]^*_p$, $\mathbf{b}^*=\frac{1}{2}[010]^*_p, \mathbf{c}^*=[001]^*_p$) unit cell with resultant $I1a1$ or $I12/a1$ space group symmetry. Indexation without the subscript p in Figs. 4 and 5 is with respect to this cell. Note that *I*-centering implies that the primitive reciprocal lattice basis vectors can be chosen to be $[110]^* \equiv \frac{1}{2}[111]^*_p$, $[011]^* \equiv \frac{1}{2}[012]^*_p$ and $[10\bar{1}]^* \equiv \frac{1}{2}[10\bar{1}]^*_p$, respectively. The simultaneous local presence of $\mathbf{G}\pm\frac{1}{2}[10\bar{1}]^*_p$ and $\mathbf{G}\pm\frac{1}{2}[101]^*_p$-type satellite reflections is thus automatically precluded as is the simultaneous presence of $\mathbf{G}\pm\frac{1}{2}[111]^*_p$-and $\mathbf{G}\pm\frac{1}{2}[1\bar{1}\bar{1}]^*_p$-type satellite reflections.

Given the initial parent *mmm* Laue symmetry and the resultant $1m1$ Laue symmetry, twinning perpendicular to $\mathbf{a}_p$ or $\mathbf{c}_p$ are the obvious candidates for the proposed twin operation (see, for example, Fig. 6). Twinning of such type can readily explain the simultaneous presence of $\mathbf{G}\pm\frac{1}{2}[10\bar{1}]^*_p$- and $\mathbf{G}\pm\frac{1}{2}[1\bar{1}\bar{1}]^*_p$-type satellite reflections in, for example, EDPs such as Fig. 5b. An HREM micrograph of an area exhibiting such a twin is shown in Fig. 7. On this micrograph two adjacent areas, indicated by white circles, show in their Fourier transforms two distinct patterns: the left-hand region exhibits only $\mathbf{G}\pm\frac{1}{2}[1\bar{1}\bar{1}]^*_p$-type satellite reflections, while the right-hand region exhibits only $\mathbf{G}\pm\frac{1}{2}[10\bar{1}]^*_p$-type satellite reflections.

Twinning of this type can also explain the presence of the strong diffuse streaking in EDPs such as that shown in Fig. 5a. Micro-twinning, i.e., twinning followed almost immediately by a further twin back to the original twin orientation, can be equivalent in the present case to a stacking fault characterized by the displacement vector $\Delta\mathbf{R}=\frac{1}{2}(\mathbf{b}+\mathbf{c})$ or, equivalently, $\frac{1}{2}$ **a** (see Fig. 6(ii)). The only reflections, **g**, that can potentially be affected by such micro-twinning are then those for which $\mathbf{g}\cdot\Delta\mathbf{R}\neq 0$ such as, for example, the heavily streaked $[1, 2k, \bar{1}]^*$ reflections of Fig. 5a but not any of the parent reflections **G** or satellite reflections

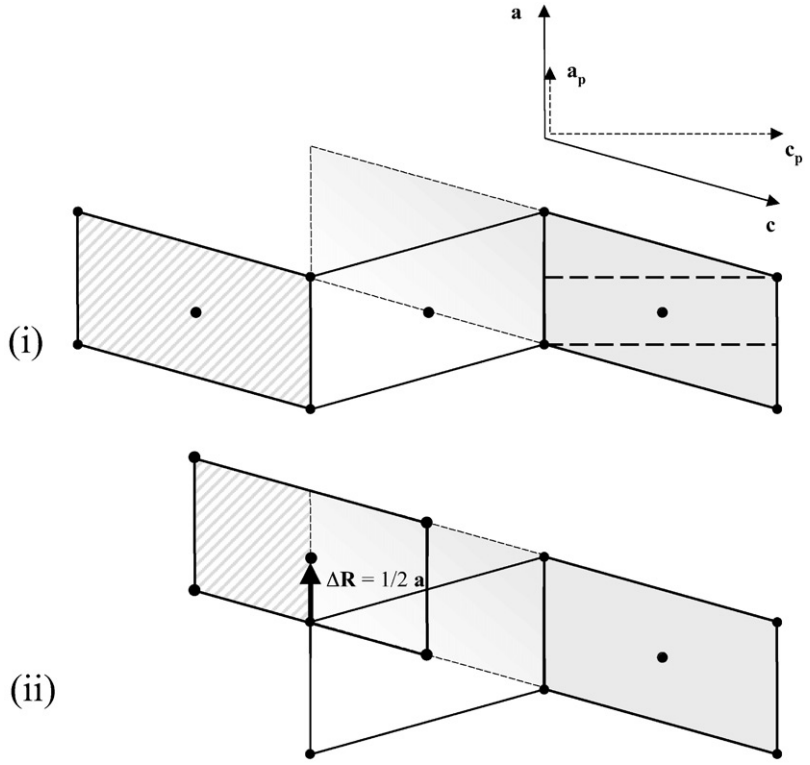

Fig. 6. Twinning models for the majority *I*1*a*1 polymorph. The parent *Bmmb* lattice vectors are shown with hatched arrows (subscript "p") at the top of the figure while those of the body-centered *I*1*a*1 superstructure are shown with solid arrows. Micro-twinning of this superstructure perpendicular to $\mathbf{a}_p$ or $\mathbf{c}_p$ can be equivalent to a stacking fault. (i) shows the original orientation of the supercell in gray (the parent cell is indicated by the hatched lines). The twinned cell is unfilled, while the striped cell has been "twinned back" and is in phase with the original cell. In (ii) the "twinned back" cell originates from the body-centered lattice point instead of from the corner. This means that it will be $\Delta\mathbf{R} = \frac{1}{2}(\mathbf{b}+\mathbf{c})$ or, equivalently, $\frac{1}{2}\mathbf{a}$, out of phase with respect to the original orientation.

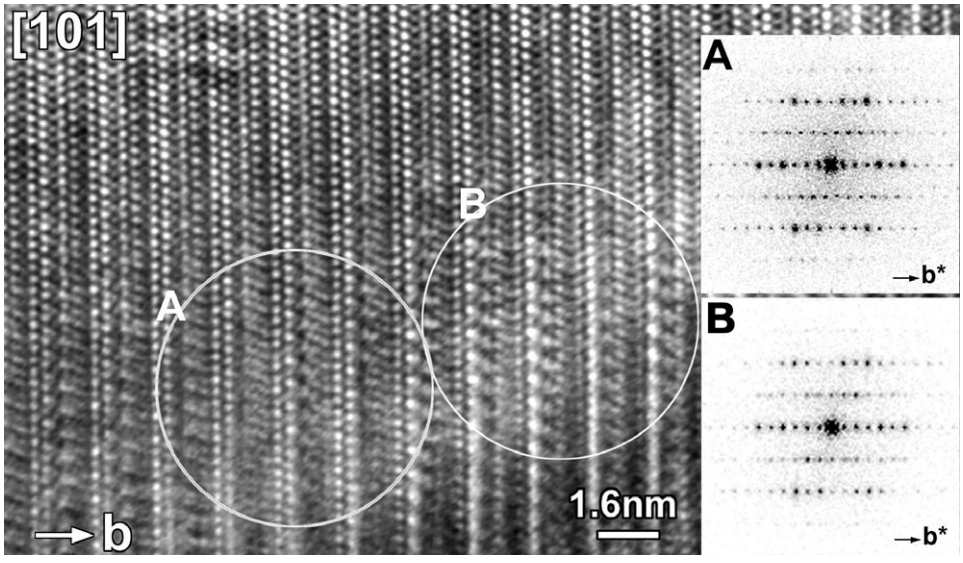

Fig. 7. Shows a real space $[101]_p$ HREM image taken from a twinned region with a corresponding EDP like that shown in Fig. 5b. The two parts of the twin are indicated by white circles. The Fourier transform of the left-hand region includes satellite reflections at $\mathbf{G}\pm\frac{1}{2}[1\bar{1}\bar{1}]^*_p$ but not at $\mathbf{G}\pm\frac{1}{2}[10\bar{1}]^*_p$, while the right hand (twinned) region includes satellite reflections at $\mathbf{G}\pm\frac{1}{2}[10\bar{1}]^*_p$ but not at $\mathbf{G}\pm\frac{1}{2}[1\bar{1}\bar{1}]^*_p$.

such as, for example, [011]* in Fig. 4a or [211]* in Fig. 5c, etc. The direction of the streaking, along **b***, requires that the plane on which the micro-twinning occurs is an (010) plane. The distribution and frequency of the twinning is then obviously responsible for the variability in appearance of nominally equivalent zone

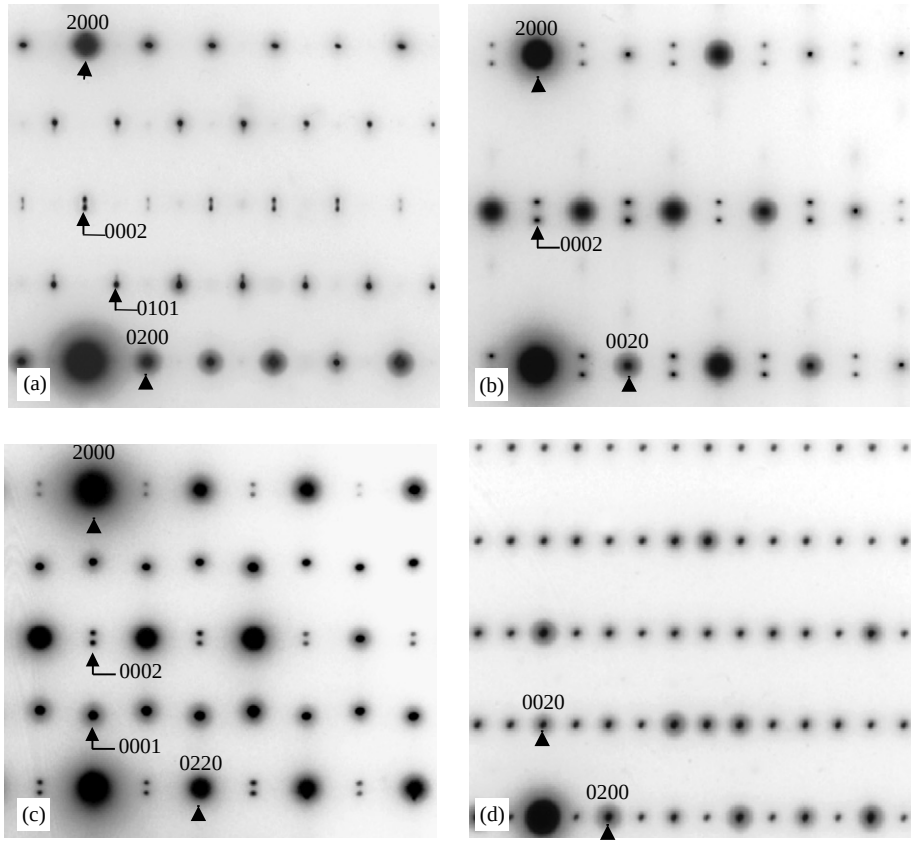

Fig. 8. Shows (a) $[001]_p$, (b) $[010]_p$, (c) $[01\bar{1}]_p$ and (d) $[100]_p$ zone axis EDPs typical of compounds from the incommensurately modulated $Ni_6(S_{1-y}Se_y)_5$ solid solution.

axis EDPs (such as those shown inFigs. 5a and b) taken with **b*** excited. Note that the variability in the scale and frequency of this (010) twinning implied by the diffraction results in this and preceding papers is going to make attempted Rietveld refinement of the structure of this polymorph rather difficult.

No other polymorph was observed in our quenched specimens despite considerable effort spent searching. This does not, however, mean that the other polymorphs reported in the literature [11,12] do not exist. They were obtained via an appropriate heating regime which it is acknowledged has not been duplicated in the current contribution.

3.3. TEM investigation of stabilized and $Ni_6(S_{1-y}Se_y)_5$ specimens

Given the difficulty in observing non-intergrown, single-phase as-quenched material in the previous section and previous results suggesting a continuous solid solution between Ni_6S_5 and Ni_6Se_5 [5], it was decided to also investigate Se-doped $Ni_6(S_{1-y}Se_y)_5$ specimens. As was perhaps to be expected, Se doping very rapidly stabilized the incommensurate interface-modulated structure type (see Fig. 3; cf., for example, Fig. 8a with Fig. 3a). All specimens examined within the $Ni_6(S_{1-y}Se_y)_5$ solid solution (i.e. $y=0.1$, 0.3, 0.5, 0.7 and 0.9) were found to contain only a single polymorph of the incommensurate interface-modulated structure type (trace amounts of Ni_3S_2 were detected for $y=0$ and 0.1 and NiSe for $y=1$ by XRPD—see Table 1). The only difference found from one composition to the next was a slight but systematic increase in the magnitude of the incommensurate primary modulation wave-vector $\mathbf{q}=(\frac{1}{2}-\varepsilon)\mathbf{a}_p^*$ from ε positive and $\sim 0.018(5)$ for $y=0.1$ to $\sim 0.008(5)$ for $y=0.5$ to zero for $y=0.7$ to $\varepsilon\sim -0.015(5)$ for $y=0.9$.

Detailed comparison of Fig. 8 with Fig. 2 of [13], however, reveals a subtle but significant difference in that the average structure space group in the current case is *Bmmb* whereas in the case of Ni_6Se_5, it was *Pmmn* [13]. The observed characteristic extinction conditions in the current case (see Fig. 8) are as follows: $F(hklm)=0$ unless $h+l$ is even requiring the average structure to be *B*-centered, $F(hk0m)=0$ unless h, $k+m$ are even (see Fig. 7a) and $F(h0lm)=0$ unless m is even (see Fig. 7b). The implied superspace group symmetry is thus at least $B2mb(\frac{1}{2}-\varepsilon,0,0)0ss$ but most probably $Bmmb(\frac{1}{2}-\varepsilon,0,0)0ss$, a non-standard setting of superspace group number 63.7 $(Amam(0,0,\frac{1}{2}-\varepsilon,)ss0$ in Table 9.8.3.5 of [15]. The

corresponding superspace generating operations can be taken to be $\{x_1+\frac{1}{2},x_2,x_3+\frac{1}{2},x_4\}$, $\{x_1,-x_2+\frac{1}{2},x_3,x_4+\frac{1}{2}\}$, $\{x_1,x_2+\frac{1}{2},-x_3,x_4+\frac{1}{2}\}$ and $\{-x_1,x_2,x_3,-x_4+2\phi\}$ respectively [16,17].

4. Conclusions

Two quite distinct polymorphs have been identified in our quenched material, a minority incommensurate interface-modulated structure polymorph which we identify with the ".. highest temperature polymorph .." of Putnis [9] and the as-quenched α^{i} polymorph of Seim et al. [12]. EDPs from this polymorph are consistent with earlier (but incomplete) diffraction evidence from both Putnis [9] and Fleet [7]. The existence of this polymorph is perhaps not surprising given that it is very closely related to the only known polymorph of $Ni_{6\pm x}Se_5$ [13] and that it is rapidly stabilized to room temperature upon doping of the sulfide with selenium (see Fig. 8).

The majority polymorph found was an $I1a1$, $\mathbf{a}=2\mathbf{a}_p$, $\mathbf{b}=2\mathbf{b}_p$, $\mathbf{c}=-\mathbf{a}_p+\mathbf{c}_p$ superstructure phase which can be identified with the ".. $2a$,$2b$,$2c$ superstructure phase .. "of Putnis [9], the monoclinic α' and α'' polymorphs of Hansen et al. [10] and the α^{ii} and probably α^{iv} polymorphs of Seim et al. [12]. Seim et al. [12] reported that ".. the monoclinic lattice of α^{iv} is probably the same as that for α^{ii} .. ". Likewise Hansen et al. [10] reported two distinct α' and α'' polymorphs with the same cell. We found no evidence for distinct polymorphic forms with this same cell although twinning perpendicular to $\mathbf{a}_p$ or $\mathbf{c}_p$ on (0 1 0) planes was found to be able to give rise to quite different-looking EDPs (cf., for example, Figs. 5a and b) dependent upon the local distribution of twin planes. No evidence for any other metastable polymorphs was found.

Acknowledgments

The ANU Electron Microscope Unit is thanked for access to facilities. We would also like to acknowledge Dr. Herman Lemmens for his collaboration on the HREM results.

References

[1] T.B. Massalski (Ed.), *Binary Alloy Phase Diagrams*, American Society for Metals, Metals Park, Ohio, 1986.
[2] D. Lundqvist, Arkiv Kemi, Mineral. Geol. 24A (21) (1947) 1.
[3] F. Grønvold, R. Møllerud, E. Røst, Acta Chem. Scand. 20 (1966) 1997.
[4] A.L.N. Stevels, Philips Res. Rep. (Suppl. 9) (1969) 1–124.
[5] K. Haugsten, E. Røst, Acta Chem. Scand. 23 (1969) 3599.
[6] E. Røst, K. Haugsten, Acta Chem. Scand. 25 (1971) 3194.
[7] M.E. Fleet, Acta Crystallogr. B. 28 (1972) 1237.
[8] G. Åkesson, E. Røst, Acta Chem. Scand. A. 29 (1975) 236.
[9] A. Putnis, Am. Mineral. 61 (1976) 322–325.
[10] V. Hansen, H. Seim, H. Fjellvåg, A. Olsen, Micron Microsc. Acta 23 (1992) 177.
[11] S. Stølen, H. Fjellvåg, F. Grønvold, H. Seim, J. Chem. Thermodyn. 26 (1994) 987.
[12] H. Seim, H. Fjellvåg, F. Grønvold, S. Stølen, J. Solid State Chem. 400 (1996) 121.
[13] L. Norén, G. van Tendeloo, R.L. Withers, J. Solid State Chem. 162 (2001) 122.
[14] M. Hart, J. Cryst. Growth 55 (1981) 409.
[15] T. Janssen, A. Janner, A. Looijenga-Vos, P.M. de Wolff, in: A.J. Wilson (ed.), *International Tables for Crystallography*, Vol. C, Kluwer Academic Publishers, Dordrecht, 1992, pp. 797–835.
[16] R.L. Withers, S. Schmid, J.G. Thompson, Prog. Solid State Chem. 26 (1998) 1.
[17] S. van Smaalen, Cryst. Rev. 4 (1995) 79.